Anisotropic dye adsorption and anhydrous proton conductivity in smectic liquid crystal networks

ACS APPLIED MATERIALS & INTERFACES

Research Article

www.acsami.org

Anisotropic Dye Adsorption and Anhydrous Proton Conductivity in Smectic Liquid Crystal Networks: The Role of Cross-Link Density, Order, and Orientation

Ting Liang,[†,‡,∥] Huub P. C. van Kuringen,[†,⊥] Dirk J. Mulder,[†,⊥] Shuai Tan,[∥] Yong Wu,[∥] Zandrie Borneman,[‡] Kitty Nijmeijer,*[,‡] and Albertus P. H. J. Schenning*[,†,§]

[†]Department of Functional Organic Materials and Devices, Chemical Engineering and Chemistry, [‡]Membrane Materials and Processes, Chemical Engineering and Chemistry, and [§]Institute for Complex Molecular Systems (ICMS), Eindhoven University of Technology, P.O. Box 513, 5600 MB Eindhoven, The Netherlands

[∥]School of Chemical Engineering, Sichuan University No. 24 South Section 1, Yihuan Road, Chengdu 610065, China

[⊥]Dutch Polymer Institute (DPI), PO Box 902, 5600 AZ Eindhoven, The Netherlands

Supporting Information

ABSTRACT: In this work, the decisive role of rigidity, orientation, and order in the smectic liquid crystalline network on the anisotropic proton and adsorbent properties is reported. The rigidity in the hydrogen-bonded polymer network has been altered by changing the cross-link density, the order by using different mesophases (smectic, nematic, and isotropic phases), whereas the orientation of the mesogens was controlled by alignment layers. Adding more cross-linkers improved the integrity of the polymer films. For the proton conduction, an optimum was found in the amount of cross-linker and the smectic organization results in the highest anhydrous proton conduction. The polymer films show anisotropic proton conductivity with a 54 times higher conductivity in the direction perpendicular to the molecular director. After a base treatment of the smectic liquid crystalline network, a nanoporous polymer film is obtained that also shows anisotropic adsorption of dye molecules and again straight smectic pores are favored over disordered pores in nematic and isotropic networks. The highly cross-linked films show size-selective adsorption of dyes. Low cross-linked materials do not show this difference due to swelling, which decreases the order and creates openings in the two-dimensional polymer layers. The latter is, however, beneficial for fast adsorption kinetics.

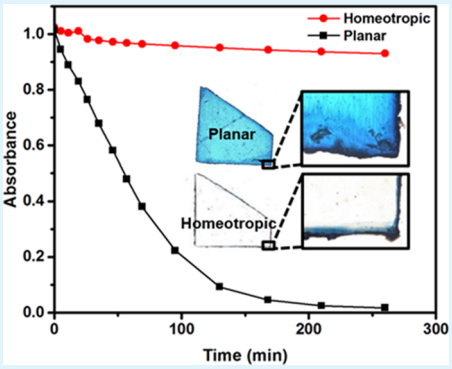

KEYWORDS: *smectic liquid crystals, liquid crystalline networks, nanoporous polymers, adsorption, proton conduction*

1. INTRODUCTION

Anisotropic nanoporous materials are currently of great interest for their applications in areas, such as filtration, adsorption, separation, ion conduction, and drug delivery.[1−6] The unique direction-dependent properties of anisotropic nanomaterials leads to significant improvements of the device performance. For example, in the case of ion-conducting materials, the transport properties are greatly improved by directional control and the conductivity can be much higher along the pore direction than perpendicular to it.[7−11] Control of the order and orientation of the building blocks in these nanomaterials is essential to control their transport properties. For such nanomaterials, well-defined highly ordered aligned self-assembled structures are required.[9−11] However, the construction of anisotropic nanomaterials remains a challenge as control over the order and orientation on large length scales is not trivial.[8,12]

Liquid crystals (LCs) have been proven to be good candidates for construction of nanoporous materials. They can be easily aligned resulting in materials with a monolithic structure on macroscopic length scales.[13−15] LCs combine the dynamic nature of liquids and the anisotropic order of crystals. Therefore, LCs are promising materials for the fabrication of anisotropic nanomaterials for ion separation, conduction, adsorption, and catalysis. So far, LC polymers with aligned nanopores have been reported that show anisotropy for ionic conduction[16−19] and highly selective separations or biodiffusion processes.[20−22] Studies to investigate the role of the molecular arrangement, order, and pore orientation, which have a decisive role in transport properties through the materials have not been reported. Such studies are important to improve and tune the functional properties of anisotropic materials.[23−25]

Previously, we reported on a nanoporous polymer based on hydrogen-bonded smectic liquid crystals that were able to very

Received: June 29, 2017
Accepted: September 22, 2017
Published: September 22, 2017

DOI: 10.1021/acsami.7b09386
ACS Appl. Mater. Interfaces 2017, 9, 35218−35225

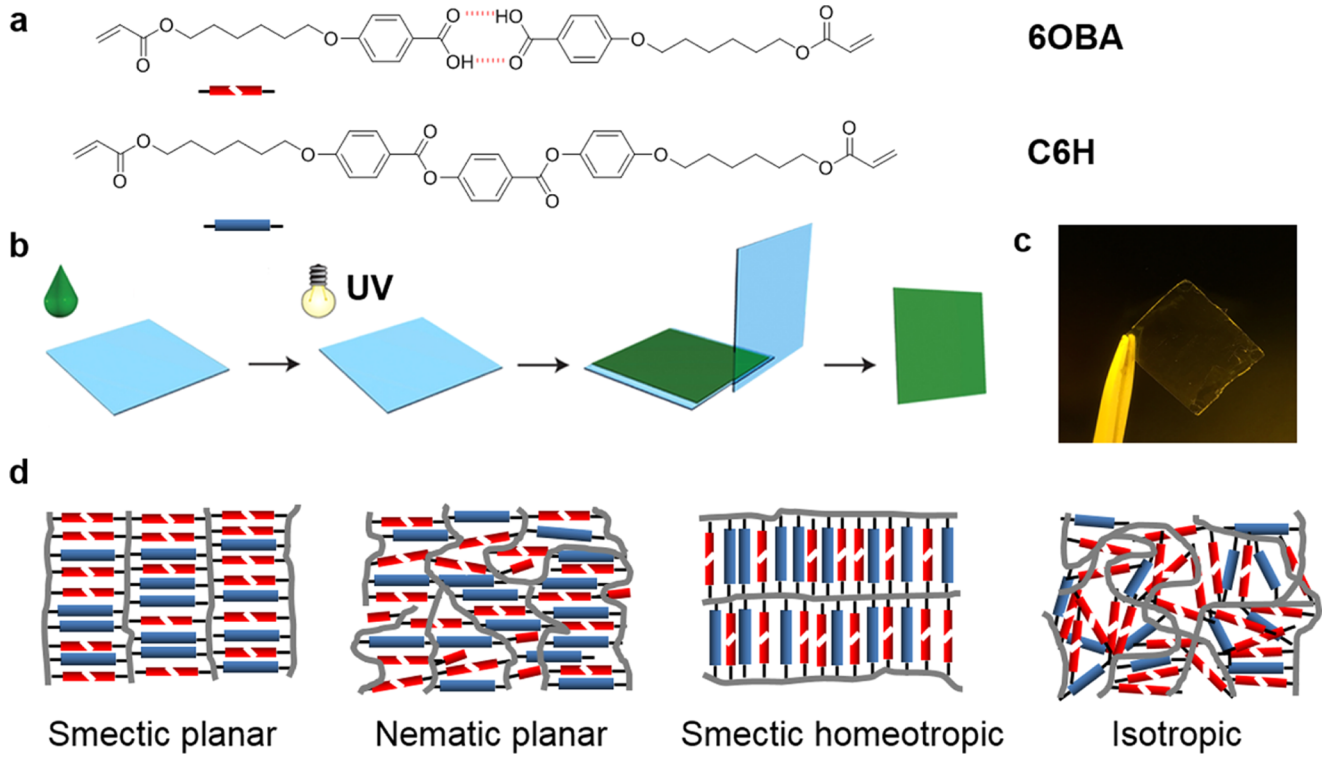

Figure 1. (a) Molecular structures of hydrogen-bonded 6OBA dimer and cross-linker C6H. The ratio between 6OBA and C6H was systematically changed from 90:10 to 50:50. (b) Schematic representation of the fabrication process to prepare the liquid crystal networks. (c) The free-standing hydrogen-bonded polymer film (6OBA−C6H (30%)). (d) Schematic representation of the hydrogen-bonded polymer networks with different LC organizations (cross-sectional area). The planar networks do have pores on the surface, whereas the homeotropic network has the pores only on the side of a film. The smectic networks possess straight pores, the nematic film has tortuous pores, whereas the isotropic polymer film has a disordered pore structure. Drawings are idealized schematic representations.

Table 1. Photopolymerization Conditions of the Different Polymer Films

alignment	planar					homeotropic
phase	smectic			nematic	isotropic	smectic
temperature (°C)	95			105	130	95
cross-linker content	10%	30%	50%	30%	30%	30%

efficiently adsorb cationic dyes[26] and on hydrogen-bonded nonpolymerized liquid crystals that exhibited anhydrous proton conduction behavior.[27] We now report on the anisotropic dye adsorption and anhydrous proton conductivity in these materials and show the crucial role of the orientation, rigidity, and order in the polymer film. The orientation and order in the polymer films are evaluated by changing the cross-link density, molecular alignment, and by using different LC phases. High anisotropic proton conductivity and size selectivity adsorption of dyes are observed in the smectic phase with an optimized cross-link density.

2. EXPERIMENTAL SECTION

2.1. Materials. The hydrogen-bridged 4-(6-acryloxy-hexyl-1-oxy)-benzoic acid (6OBA, Figure 1a) and the LC cross-linker, 4-((4-(6-(acryloyloxy)hexyloxy)phenoxy)carbonyl)phenyl 4-(6-(acryloyloxy)-hexyloxy)benzoate (C6H, Figure 1a) were both custom made by Synthon Chemicals, Germany. The initiator 1-hydroxycyclohexyl phenylketone (Irgacure 184) was supplied by Ciba Specialty Chemicals and inhibitor *p*-methoxyphenol was purchased from Aldrich. Methylene blue (MB) was purchased from Acros Organics, whereas the fluorescein-labeled methylated poly(propylene imine) dendrimer of generation 3 (Me-G3-PPI) was supplied by SyMO-Chem BV.

2.2. Preparation of the Liquid Crystalline Network. LC mixtures were made with different amounts of 6OBA and C6H (10−50 wt %), 0.5 wt % 1-hydroxycyclohexyl phenylketone as the photoinitiator, and 0.1 wt % of *p*-methoxyphenol as the inhibitor. The compounds were dissolved in tetrahydrofuran, which was subsequently evaporated. The membranes with a thickness of 20 μm were made by processing the mixture in the isotropic phase at 110 °C by capillary suction between two accurately spaced glass plates. To obtain planar alignment, the glass plates were provided with rubbed polyimide (Optmer AL 1051; JSR Corporation, Tokyo, Japan). The photopolymerization in the smectic LC state of the monomer mixture was performed at 95 °C for 5 min with a mercury lamp (OmniCure s1000), with an intensity of approximately 5 mW cm^{-2} at the sample surface, followed by a heat treatment of 15 min at 135 °C to ensure full conversion of the acrylate groups.[26] The photopolymerization in the nematic phase and for the isotropic sample were similarly processed as that in the smectic phase but performed at 105 and 130 °C, respectively. For homeotropic alignment, octadecyltrimethoxysilane-functionalized glass cells were used and the films were similarly processed, as the planar alignment films described before. Table 1 shows the photopolymerization conditions of the different films.

2.3. Characterization. Differential scanning calorimetry (DSC) measurements were performed in hermetic T zero aluminum sample pans under a nitrogen atmosphere using a TA Instruments Q1000 DSC equipped with an RCS90 cooling accessory. The DSC experiments were conducted at a rate of 10 °C min^{-1}. Polarized

DOI: 10.1021/acsami.7b09386
ACS Appl. Mater. Interfaces 2017, 9, 35218−35225

optical microscopy (POM) studies were conducted using a Leica CTR 6000 microscope equipped with two polarizers that are operated crossed with the sample in between, a Linkam hot stage THMS600 with a Linkam TMS94 controller and a Leica DFC420 C camera. Fourier transform infrared (FTIR) spectra were obtained using an FTS 6000 spectrometer from Bio-Rad equipped with Specac Golden Gate diamond attenuated total reflectance and were signal-averaged over 50 scans at a resolution of 4 cm^{-1}. Thermogravimetric analyses (TGA) were performed on a TA Instruments Q500 TGA in a nitrogen atmosphere till 600 °C. Samples were heated at a rate of 10 °C min^{-1}. Optical retardation measurements were performed with a polarization microscope (Leica DMLP) equipped with a tilting quartz plate compensator. The microscope was provided with a hot stage to measure the effect of temperature. X-ray diffraction (XRD) (wide-angle X-ray scattering and medium-angle X-ray scattering) of the polymer films were performed on a Ganesha lab instrument equipped with a GeniX-Cu ultralow divergence source, producing X-ray photons with a wavelength of 1.54 Å and a flux of 1 × 108 ph s^{-1}. Scattering patterns were collected using a Pilatus 300 K silicon pixel detector with 487 × 619 pixels of 172 μm^2 in size. XRD measurements at wide angles on polymer films containing different ratios of 6OBA−C6H were performed at the DUBBLE-BM26B beamline at ESRF, Grenoble, France.[28,29]

2.4. Anhydrous Proton Conduction. Electrochemical impedance spectroscopy (EIS) was recorded using an Autolab potentiostat equipped with a hot stage in the frequency range from 10 mHz to 1 MHz (applied voltage: 10 mV). Polymer films were prepared in the commercial liquid crystal cells supplied by Instec, Inc., Boulder, Colorado. For planar and homeotropic aligned samples, LC2-5.0 and S100A183Ut180 glass cells were used, respectively. Indium tin oxide areas in the center of the cell were used as electrodes. The conductivities were measured as a function of temperature between 100 and 230 °C with 5 °C intervals. Before the measurements, the polymer films were vacuum-dried overnight at room temperature. The impedance spectrum was modeled as an equivalent circuit and divided into imaginary (Z'') and real (Z') components. The resistance (R_b) was estimated from the intersection of the real axis (Z') and the semicircle of the impedance spectrum. The proton conductivities σ were calculated using eq 1

$$\sigma = \frac{d}{R_b A} \tag{1}$$

where d is the thickness of the film, A is the area of the film, and R_b is the resistance of the sample to conduction (Ω).

2.5. Dye Adsorption. Before the adsorption process, the hydrogen-bonded polymer films were immersed in 5 mL 0.1 M KOH solution varying from 15 min to 1 day to deprotonate the carboxylic acid moieties. This resulted in rupture of the hydrogen bridges and formation of the polymer salt with open pores. The exposure time was dependent on the cross-link density. The adsorption measurements were carried out by using freshly made aqueous cationic dye solutions of MB and Me-G3-PPI.[30] The cuvettes were equipped with a magnetic stirring bar. The MB adsorption experiments were carried out using 3 mL of MB solution (5.0 μg mL^{-1}, 15.6 μM) and millimeter-sized films with milligram weight. The adsorption process was followed using a UV−vis spectrophotometer. The maximum of the MB absorbance at 665 nm was used to investigate the depletion of MB in solution. Dendrimer adsorption experiments were performed with 3 mL of 0.1 mg mL^{-1} (1.51×10^{-4} M) Me-G3-PPI and polymer adsorbents with 1.09×10^{-5} mol of adsorption sites. This was a one-, twofold excess of cationic groups over anionic adsorption sites. The adsorption process was followed by measuring the maximum absorbance of fluorescein at 494 nm over time. The amount of adsorbed dye was calculated as described before[26] by using eq 2

$$q = \frac{(c_i - c_f)V}{n_m} \times 100\% \tag{2}$$

where q (mol mol^{-1}) is the amount of dye per amount of carboxylate moieties in the polymer film, c_i and c_f (mol L^{-1}) are the concentrations of dye in solution before and after adsorption, respectively, V (L) is the volume of the dye solution, and n_m (mol) was the amount of carboxylate moieties.

3. RESULTS AND DISCUSSION

3.1. Preparation and Characterization of Liquid Crystalline Networks. To study the role of the rigidity, order, and orientation, the liquid crystalline mixture with up to 50% cross-linker was incorporated in liquid crystal cells having different alignment layers. The LC mixtures were photopolymerized at different temperatures, and after thermal postpolymerization and opening of the cells, free-standing films with different locked-in mesophases (order), cross-link densities (rigidity), and different molecular orientations were obtained (Figure 1). FTIR measurements reveal full conversion of the acrylate moieties (Figure S1)

The alignment and organization of the polymerized films were further investigated with POM measurements (Figures S2 and S3). In all cases, LCs are well aligned along the rubbing direction. Planar alignment samples reveal dark images under parallel conditions, and bright images under 45° tilt reveal birefringent polymer films. In the case of the homeotropically aligned films, dark images were obtained at all angles. XRD measurements showed the influence of cross-link density on the layer spacing and tilt angle in the smectic liquid crystalline networks. The results indicate that adding cross-linker up to 30% does not increase the layer spacing further because the rise in the layer spacing is caused by the decrease of the molecular tilt (Figures S4 and S5). Therefore, the channels in the highly cross-linked films are straighter than those in the lower cross-linked membranes. TGA measurements show that the 6OBA−C6H polymer films are fully polymerized and stable up to 400 °C (Figure S6a). The optical retardation, being the product of birefringence Δn and film thickness d, showed that only the optical retardation suddenly drops to a low value for the low cross-linked smectic polymer films (C6H 10%) at about 180 °C, implying a loss of the smectic order (Figure S6b).[31] The DSC measurement of 6OBA−C6H (10%) polymer film (Figure S6c) shows a phase transition peak at 178 °C, whereas in the higher cross-linked films, no clear phase transition peaks are observed. Temperature-dependent FTIR measurements indicate that the hydrogen bond interactions break at around 180 °C (Figure S1).

To apply the smectic liquid crystalline networks as absorbents, the polymer films have to be converted to the polymer salt by immersing them in a KOH solution. Interestingly, the opening of the pores in the homeotropic polymer network starts on the outer side of the film (Figure S7a). FTIR revealed that the edge showed the conversion of the hydrogen-bonded carboxylic acids to the carboxylate salt (Figure S7b), whereas in the middle of the films no conversion is observed. This suggests that the conversion starts at the edge. During base treatment, swelling of the films was observed. As observed earlier, in the parallel direction, no swelling was observed in the low and high cross-link density films. Interestingly, shrinkage was observed for samples with an intermediate cross-link density, which indicates a reduction of the smectic layer spacing (vide infra). Increasing the amount of C6H cross-linker shows gradually less swelling in the perpendicular direction and reaches marginal swelling for the films containing 50% cross-linker (Figure S8). The increased

DOI: 10.1021/acsami.7b09386
ACS Appl. Mater. Interfaces 2017, 9, 35218−35225

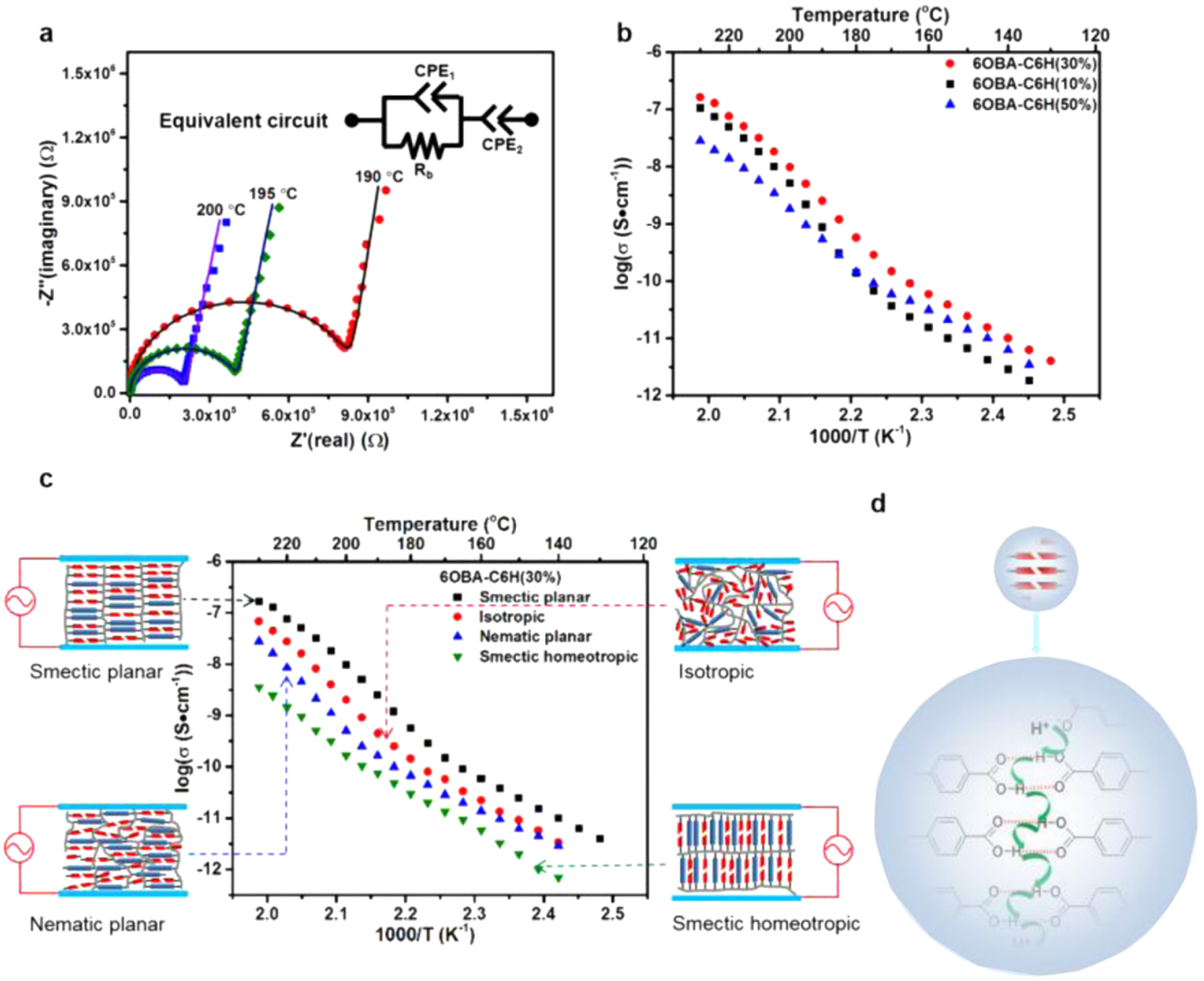

Figure 2. (a) Nyquist plots of the smectic planar aligned 6OBA−C6H (30%) polymer film at 190, 195, and 200 °C. (b) Anhydrous proton conductivities of 6OBA−C6H polymer films with different amounts of C6H. (c) Anhydrous proton conductivities as a function of the temperature of the smectic planar, nematic planar, isotropic, and smectic homeotropic 6OBA−C6H (30%) polymer films. (d) Schematic illustration of proton transfer pathway in a smectic 6OBA−C6H polymer film.

cross-link density gives the carboxylate tethers possibly less freedom to spread within the layer. Furthermore, the hydrophilicity of the network is changed due to cross-linking. This can cause lower water adsorption. Moreover, the increased cross-link density also improves the mechanical integrity of the porous films but this was not further quantified. POM pictures of the polymer salt films show textures similar to those in the hydrogen-bonded state, indicating that the network is maintained, thanks to the higher cross-link density (Figures S9 and S10). The high LC cross-link density is able to fixate the molecular orientation of the cross-linker better, but the nonbridged carboxylate tethers are probably still randomly orientated.[31] XRD measurements showed that increasing the amount of cross-linkers resulted in more anisotropic diffraction patterns (Figure S11a), both for the intermolecular distance and for the smectic layer spacing. The highly cross-linked samples revealed distinguishable smectic diffraction signals, indicating that a higher cross-link density is beneficial for maintaining the alignment and order. Interestingly, the smectic layer spacing is 3.5 ± 0.1 nm for all cross-link densities (Figure S11b). This means that the cross-link density does not influence the layer spacing in the humid polymer salt films. For the high cross-linked materials (30−50% cross-linker), this means a layer spacing decrease of 10% in comparison with the hydrogen-bonded samples before the alkaline treatment. Interestingly, on a macroscopic scale, shrinkage of about 10% was observed in the direction perpendicular to the layers, which indeed corresponds to the reduction in layer spacing. On the basis of the swelling, from POM and XRD data, we can conclude that a high cross-link density prevents the swelling almost completely and is also able to keep the alignment of the cross-linkers to a large extent (Figure S7c). XRD points to more orientation of the carboxylate tethers, whereas the birefringence suggests no alignment of the tethers.

Because of their ordered, well-defined nanoporous structure, the developed liquid crystal films are promising candidates, for example, for fuel cell applications and selective separation processes. As a first evaluation of their potential for such applications, proton conductivity and dye adsorption characteristics of the films were determined.

3.2. Anhydrous Proton Conduction. Anhydrous proton conductivity was measured by alternating current impedance

DOI: 10.1021/acsami.7b09386
ACS Appl. Mater. Interfaces 2017, 9, 35218−35225

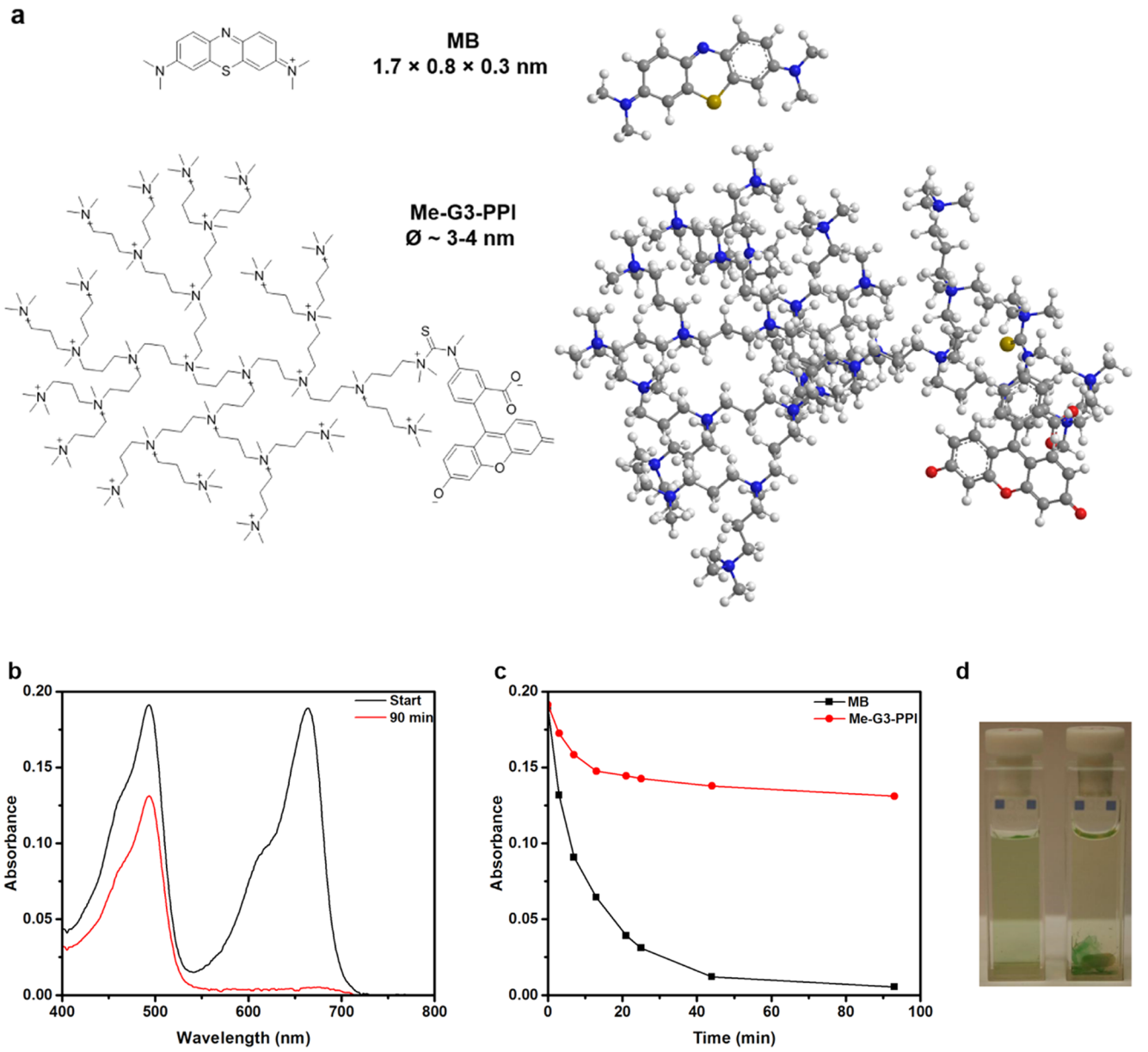

Figure 3. (a) Two cationic dyes used in this research. Methylene blue (MB) is used to resemble small molecules. MB has a size of 1.7 × 0.8 × 0.3 nm^3. The fluorescein-labeled methylated poly(propylene imine) dendrimer of generation 3 (Me-G3-PPI) was used as large spherical cation, with a size of approximately 3−4 nm. (b) UV−vis spectrum of the initial dye mixture and after 90 min of adsorption. (c) Adsorption kinetics of both dyes. (d) Photograph of the dye solution before and 90 min after adding the polymer films (6OBA−C6H (50%)).

from 100 to 230 °C using the hydrogen-bonded 6OBA−C6H films with different C6H content (10, 30, and 50%, respectively). Figure 2a shows a typical impedance response (Cole−Cole plots) at 190, 195, and 200 °C, respectively.

Subsequently, the proton conductivities of all three films were measured as a function of temperature (Figure 2b). For all films, the conductivities increase upon increasing the temperature and the 6OBA−C6H (30%) film shows the highest conductivity. In these polymer films, the protons hop along the aligned channels formed by the dimer structure between two benzoic acid (6OBA) molecules (Figure 2d). The anhydrous proton conductivity was determined by the proton bulk density and the order in the polymer film. The straight channels in the higher cross-linked films (Figure S5a) favor the proton conduction because straight channels have the shortest path length and lowest tortuosity.[32] As discussed previously, cross-linker content higher than 30% does not change the structure any further (Figure S5). The order of the 6OBA−C6H (30 and 50%) is the same. The 6OBA−C6H (30%) film has, however, a higher proton content and therefore the highest conductivity.

The smectic planar films show the highest conductivities over the whole temperature range, revealing that an oriented ordered hydrogen-bonded liquid crystal favors proton conductivity. Remarkably, the proton conduction in the isotropic ordered sample is higher than in the nematic ordered film. Likely, disordered molecules in isotropic ordered films provide randomly tortuous paths, leading to better conduction than in nematic ordered samples in which the channels are separated by the aliphatic chains, which is in agreement with the findings of Ichikawa et al.[33]

To explore the role of the pore orientation, proton conductivity measurements were carried out using the smectic

DOI: 10.1021/acsami.7b09386
ACS Appl. Mater. Interfaces 2017, 9, 35218−35225

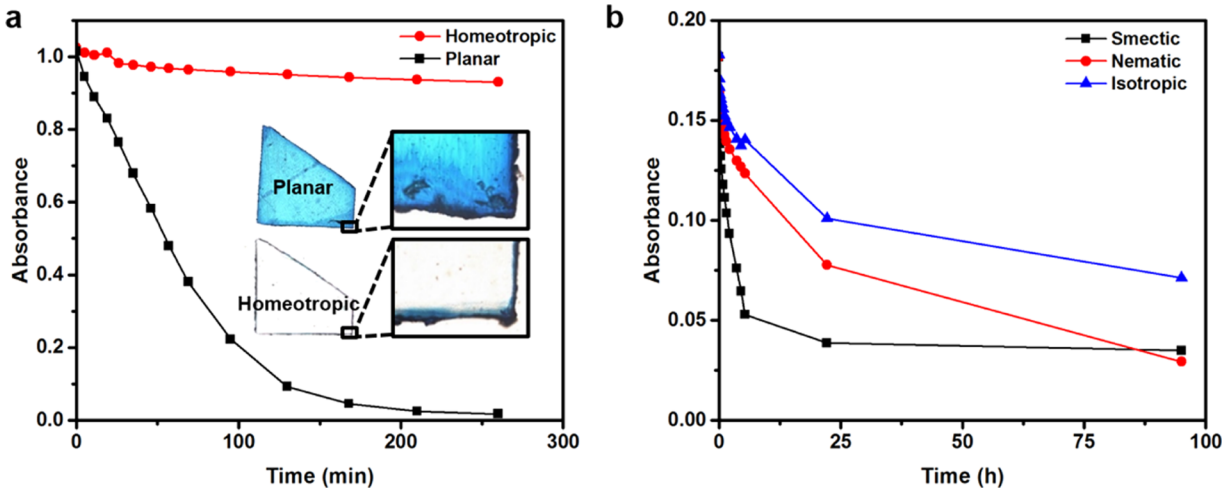

Figure 4. (a) Adsorption kinetics and microscopy pictures of the MB adsorption in planar and homeotropic aligned smectic LC polymer salt networks (6OBA−C6H (50%)). (b) Adsorption kinetics of the larger Me-G3-PPI adsorption in the smectic, nematic, and isotropic 6OBA−C6H (50%) LC polymer salt network.

planar and homeotropic aligned 6OBA−C6H (30%) polymer films. In the case of the planar aligned samples, the proton channels are oriented in the direction of the electrodes, whereas in the homeotropic samples, the channels are perpendicular to the direction of current flow and proton conductivity is diminished. The proton conductivity of the planar aligned sample is 54 times higher than that of the homeotropic aligned film (Figure 2c), revealing anisotropic proton conduction.

3.3. Dye Adsorption. The influence of the increased cross-link density on the adsorption characteristics was investigated by comparing porous LC polymers with 10 and 50% cross-linkers. The polymer films in their salt form were either exposed to the small dye, methylene blue (MB) or to the larger dye, yellow fluorescein-labeled methylated third generation poly(propylene imine) dendrimer (Me-G3-PPI) (Figure 3a).[26] After adding the MB or Me-G3-PPI, both films become colored, that is, blue or yellow, indicating the adsorption of both dyes. This means that the increased LC cross-link density cannot prevent the adsorption of MB or Me-G3-PPI. The adsorption kinetics (Supporting Information) reveal, however, notable differences between the low and the highly cross-linked network. The adsorption in the highly cross-linked network is slower and does not follow pseudo-second order kinetics (R^2 (MB) = 0.952). This is probably the result of the decreased swelling, resulting in less pore volume and the more rigid network structure (vide supra). The adsorption kinetics for MB are slightly reduced, whereas for Me-G3-PPI, adsorption is much slower than for the low cross-linked network. This indicates that the cross-link density plays an important role in the adsorption of bigger cations. However, after approximately 1 day (1360 min) of adsorption, this network was also able to adsorb the same amount of Me-G3-PPI as the 10% network. Both the low and the highly cross-linked films reached an occupation degree of 97 ± 3% (Figure S12). Because the carboxylate moieties act as the adsorption sites, this means that approximately all adsorption sites are occupied with a cationic charge of Me-G3-PPI.[26] Despite the fact that enhanced discrimination based on size is not achieved in the experiments mentioned above, the difference in kinetics does allow size-selective adsorption. When a 50% polymer film in its salt form with an excess of adsorption sites is added to a mixture solution of MB and Me-G3-PPI, the film becomes blue. The network adsorbs MB much faster than it adsorbs Me-G3-PPI. After 90 min, all MB is adsorbed, whereas only 30 % of the Me-G3-PPI is adsorbed (Figure 3).

To explore the role of the pore orientation and the existence of pore openings in the polymer layers, adsorption experiments were carried out using low and highly cross-linked smectic homeotropic and planar aligned networks and MB as a dye. For both films, the low cross-linked network 6OBA−C6H (10%) does not show anisotropic adsorption behavior (Figure S13a). Also the adsorption kinetics of the planar and homeotropic film are the same (Figure S13b). This is probably the consequence of the low cross-link density and the severe anisotropic swelling that results in the low order in the material. The swelling creates space in between the polymer chains in the two-dimensional (2D) polymer layer, resulting in openings that create transverse connections between the pores and allow lateral in-diffusion of the dye,[26] independent of the organization of the crystals. This means that the pores are interconnected, which is beneficial for the rate of adsorption. Furthermore, both films are homogeneously colored. Only the edges of both films are slightly more colored, which is most probably caused by edge roughness and/or cutting deformations (Figure S13a, inset). In contrast to this, the adsorption in the highly cross-linked networks 6OBA−C6H (50%) reveals large differences between the different molecular organizations (Figure 4a). Adsorption in the homeotropic aligned network is much slower. Even after 1 day, this network shows no adsorption, whereas the planar network reaches a high adsorption equilibrium state after only a few hours. These highly cross-linked networks have a more ordered structure and almost no swelling, resulting in ordered pores and anisotropic adsorption. At the early stage of the adsorption process, microscopy pictures show that the homeotropic film is primarily colored at the edges (Figure 4a, inset). After longer adsorption time, the films become light blue. In the planar aligned sample, the chevron structure is visible without the use of polarizers, at high magnification, by a staining-like process of the dye into the oblique pores.

The influence of the pore structure on the adsorption kinetics is investigated with the highly cross-linked networks having a smectic planar, nematic planar, and isotropic organization. MB adsorption reveals minimal differences

DOI: 10.1021/acsami.7b09386
ACS Appl. Mater. Interfaces 2017, 9, 35218−35225

between the smectic and nematic phase, whereas the isotropic phase is slightly slower (Figure S13b). This means that the pore structure is of less importance for the adsorption of small ions such as MB. The adsorption of the larger Me-G3-PPI dye revealed a large effect (Figure 4b). The adsorption in the isotropic network is the slowest, followed by the nematic phase, whereas the smectic phase is the fastest. This is most likely the result of the decreasing tortuosity and a better-defined pore structure. The straight pores in the smectic network promote fast adsorption, whereas a more disordered pore structure increases the path length and slows down adsorption.

4. CONCLUSIONS

We studied the role of rigidity, orientation, and order in the adsorption and conduction properties of hydrogen-bonded smectic liquid crystalline networks. The results showed that the addition of more cross-linkers improves the integrity of the polymer films, resulting in more ordered 2D nanostructures and a higher conductivity and a higher adsorption selectivity. Straight and short paths favor the proton conduction and adsorption greatly. The anisotropic films exhibit anisotropic proton conduction and adsorption. Moreover, the ordered layer structures of the smectic LC networks are favored over the disordered structures in nematic and isotropic networks. Although the proton conductivities are low ($\sim 10^{-7}$ S cm^{-1}), the polymer films show anisotropic proton conductivity with a 54 times higher conductivity in the direction perpendicular to the molecular director. The highest absorption kinetics and capacity with occupation degree close to 100% is observed for the smectic ordered polymers having straight lamellar pores. Our results show the crucial role of lamellar order, orientation, and cross-link density in the fabrication of anisotropic nanomaterials. It gives design rules to fabricate polymers with enhanced and anisotropic functional properties.

■ ASSOCIATED CONTENT

Supporting Information

The Supporting Information is available free of charge on the ACS Publications website at DOI: 10.1021/acsami.7b09386.

Fabrication, characterizations of the polymer films; conductivity and adsorption data of the polymer films (PDF)

■ AUTHOR INFORMATION

Corresponding Authors

*E-mail: D.C.Nijmeijer@tue.nl (K.N.).
*E-mail: A.P.H.J.Schenning@tue.nl (A.P.H.J.S.).

ORCID

Kitty Nijmeijer: 0000-0002-1431-2174
Albertus P. H. J. Schenning: 0000-0002-3485-1984

Notes

The authors declare no competing financial interest.

■ ACKNOWLEDGMENTS

T.L. is financially supported by China Scholarship Council (CSC). This research forms part of the research program of the Dutch Polymer Institute (DPI), projects 742 and 776. The authors would like to thank Dick Broer for the fruitful discussions and Dr. Lu Gao for the EIS measurements and discussion.

■ REFERENCES

(1) Xia, Y.; Yang, P.; Sun, Y.; Wu, Y.; Mayers, B.; Gates, B.; Yin, Y.; Kim, F.; Yan, H. One-Dimensional Nanostructures: Synthesis, Characterization, and Applications. *Adv. Mater.* **2003**, *15*, 353−389.
(2) Kato, T. From Nanostructured Liquid Crystals to Polymer-Based Electrolytes. *Angew. Chem., Int. Ed.* **2010**, *49*, 7847−7848.
(3) Baker, R. W. *Membrane Technology and Applications*, 3rd ed.; John Wiley & Sons, Ltd. Publications: California, 2012.
(4) Goriparti, S.; Miele, E.; De Angelis, F.; Di Fabrizio, E.; Zaccaria, R. P.; Capiglia, C. Review on Recent Progress of Nanostructured Anode Materials for Li-Ion Batteries. *J. Power Sources* **2014**, *257*, 421−443.
(5) Song, M.-K.; Park, S.; Alamgir, F. M.; Cho, J.; Liu, M. Nanostructured Electrodes for Lithium-Ion and Lithium-Air Batteries: The Latest Developments, Challenges, and Perspectives. *Mater. Sci. Eng., R* **2011**, *72*, 203−252.
(6) Alberti, G.; Casciola, M.; Pica, M.; Di Cesare, G. Preparation of Nano-Structured Polymeric Proton Conducting Membranes for Use in Fuel Cells. *Ann. N. Y. Acad. Sci.* **2003**, *984*, 208−225.
(7) Majewski, P. W.; Gopinadhan, M.; Osuji, C. O. Understanding Anisotropic Transport in Self-Assembled Membranes and Maximizing Ionic Conductivity by Microstructure Alignment. *Soft Matter* **2013**, *9*, 7106.
(8) Thorkelsson, K.; Bai, P.; Xu, T. Self-Assembly and Applications of Anisotropic Nanomaterials: A Review. *Nano Today* **2015**, *10*, 48−66.
(9) Sajanlal, P. R.; Sreeprasad, T. S.; Samal, A. K.; Pradeep, T. Anisotropic Nanomaterials: Structure, Growth, Assembly, and Functions. *Nano Rev.* **2011**, *2*, 5883−5944.
(10) Yoon, M.; Suh, K.; Kim, H.; Kim, Y.; Selvapalam, N.; Kim, K. High and Highly Anisotropic Proton Conductivity in Organic Molecular Porous Materials. *Angew. Chem., Int. Ed.* **2011**, *50*, 7870−7873.
(11) Karmakar, A.; Illathvalappil, R.; Anothumakkool, B.; Sen, A.; Samanta, P.; Desai, A. V.; Kurungot, S.; Ghosh, S. K. Hydrogen-Bonded Organic Frameworks (HOFs): A New Class of Porous Crystalline Proton-Conducting Materials. *Angew. Chem., Int. Ed.* **2016**, *55*, 10667−10671.
(12) Li, Q. *Anisotropic Nanomaterials: Preparation, Properties, and Applications*; Springer International Publishing: Switzerland, 2015.
(13) Martínez-Felipe, A. Liquid Crystal Polymers and Ionomers for Membrane Applications. *Liq. Cryst.* **2011**, *38*, 1607−1626.
(14) Funahashi, M.; Shimura, H.; Yoshio, M.; Kato, T. Functional Liquid-Crystalline Polymers for Ionic and Electronic Conduction. *Struct. Bonding* **2008**, *128*, 151−179.
(15) Broer, D. J.; Bastiaansen, C. M. W.; Debije, M. G.; Schenning, A. P. H. J. Functional Organic Materials Based on Polymerized Liquid-Crystal Monomers: Supramolecular Hydrogen-Bonded Systems. *Angew. Chem., Int. Ed.* **2012**, *51*, 7102−7109.
(16) Lee, J. H.; Han, K. S.; Lee, J. S.; Lee, A. S.; Park, S. K.; Hong, S. Y.; Lee, J.-C.; Mueller, K. T.; Hong, S. M.; Koo, C. M. Facilitated Ion Transport in Smectic Ordered Ionic Liquid Crystals. *Adv. Mater.* **2016**, *28*, 9301−9307.
(17) Ramón-Gimenez, L.; Storz, R.; Haberl, J.; Finkelmann, H.; Hoffmann, A. Anisotropic Ionic Mobility of Lithium Salts in Lamellar Liquid Crystalline Polymer Networks. *Macromol. Rapid Commun.* **2012**, *33*, 386−391.
(18) Yang, X.; Tan, S.; Liang, T.; Wei, B.; Wu, Y. A Unidomain Membrane Prepared from Liquid-Crystalline Poly(pyridinium 4-Styrene Sulfonate) for Anhydrous Proton Conduction. *J. Membr. Sci.* **2017**, *523*, 355−360.
(19) Tan, S.; Wang, C.; Wu, Y. Anisotropic Assembly of a Side Chain Liquid Crystal Polymer Containing Sulfoalkoxy Groups for Anhydrous Proton Conduction. *J. Mater. Chem. A* **2013**, *1*, 1022−1025.
(20) Long, P.; Yan, H.; Guo, X.; Hao, J. Lyotropic Liquid Crystal Phases of Lithium Perfluorinated Fatty Acid Salts in Aqueous Solutions and Molecular Dynamics Study of the Lamellar Phase. *J. Fluorine Chem.* **2012**, *135*, 315−322.

DOI: 10.1021/acsami.7b09386
ACS Appl. Mater. Interfaces 2017, 9, 35218−35225

(21) Vallooran, J. J.; Negrini, R.; Mezzenga, R. Controlling Anisotropic Drug Diffusion in Lipid–Fe_3O_4 Nanoparticle Hybrid Mesophases by Magnetic Alignment. *Langmuir* **2013**, *29*, 999–1004.
(22) Tousley, M. E.; Feng, X.; Elimelech, M.; Osuji, C. O. Aligned Nanostructured Polymers by Magnetic-Field-Directed Self-Assembly of a Polymerizable Lyotropic Mesophase. *ACS Appl. Mater. Interfaces* **2014**, *6*, 19710–19717.
(23) Kallem, P.; Eguizabal, A.; Mallada, R.; Pina, M. P. Constructing Straight Polyionic Liquid Microchannels for Fast Anhydrous Proton Transport. *ACS Appl. Mater. Interfaces* **2016**, *8*, 35377–35389.
(24) Kerr, R. L.; Edwards, J. P.; Jones, S. C.; Elliott, B. J.; Gin, D. L. Effect of Varying the Composition and Nanostructure of Organic Carbonate-Containing Lyotropic Liquid Crystal Polymer Electrolytes on Their Ionic Conductivity. *Polym. J.* **2016**, *48*, 635–643.
(25) Wen, Q.; Yan, D.; Liu, F.; Wang, M.; Ling, Y.; Wang, P.; Kluth, P.; Schauries, D.; Trautmann, C.; Apel, P.; Guo, W.; Xiao, G.; Liu, J.; Xue, J.; Wang, Y. Highly Selective Ionic Transport through Subnanometer Pores in Polymer Films. *Adv. Funct. Mater.* **2016**, *26*, 5796–5803.
(26) van Kuringen, H. P. C.; Eikelboom, G. M.; Shishmanova, I. K.; Broer, D. J.; Schenning, A. P. H. J. Responsive Nanoporous Smectic Liquid Crystal Polymer Networks as Efficient and Selective Adsorbents. *Adv. Funct. Mater.* **2014**, *24*, 5045–5051.
(27) Liang, T.; Wu, Y.; Tan, S.; Yang, X.; Wei, B. Enhancing Proton Conduction via Doping of Supramolecular Liquid Crystals (4-Alkoxybenzoic Acids) with Imidazole. *Chem. Phys. Lett.* **2015**, *637*, 22–25.
(28) Bras, W.; Dolbnya, I. P.; Detollenaere, D.; van Tol, R.; Malfois, M.; Greaves, G. N.; Ryan, A. J.; Heeley, E. Recent Experiments on a Combined Small-Angle/Wide-Angle X-Ray Scattering Beam Line at the ESRF. *J. Appl. Crystallogr.* **2003**, *36*, 791–794.
(29) Portale, G.; Cavallo, D.; Alfonso, G. C.; Hermida-Merino, D.; van Drongelen, M.; Balzano, L.; Peters, G. W. M.; Goossens, J. G. P.; Bras, W. Polymer Crystallization Studies under Processing-Relevant Conditions at the SAXS/WAXS DUBBLE Beamline at the ESRF. *J. Appl. Crystallogr.* **2013**, *46*, 1681–1689.
(30) Bögels, G. M.; van Kuringen, H. P. C.; Shishmanova, I. K.; Voets, I. K.; Schenning, A. P. H. J.; Sijbesma, R. P. Selective Absorption of Hydrophobic Cations in Nanostructured Porous Materials from Crosslinked Hydrogen-Bonded Columnar Liquid Crystals. *Adv. Mater. Interfaces* **2015**, *2*, No. 1500022.
(31) Gonzalez, C. L.; Bastiaansen, C. W. M.; Lub, J.; Loos, J.; Lu, K.; Wondergem, H. J.; Broer, D. J. Nanoporous Membranes of Hydrogen-Bridged Smectic Networks with Nanometer Transverse Pore Dimensions. *Adv. Mater.* **2008**, *20*, 1246–1252.
(32) Peckham, T. J.; Schmeisser, J.; Rodgers, M.; Holdcroft, S. Main-Chain, Statistically Sulfonated Proton Exchange Membranes: The Relationships of Acid Concentration and Proton Mobility to Water Content and Their Effect upon Proton Conductivity. *J. Mater. Chem.* **2007**, *17*, 3255–3268.
(33) Ichikawa, T.; Yoshio, M.; Hamasaki, A.; Kagimoto, J.; Ohno, H.; Kato, T. 3D Interconnected Ionic Nano-Channels Formed in Polymer Films: Self-Organization and Polymerization of Thermotropic Bicontinuous Cubic Liquid Crystals. *J. Am. Chem. Soc.* **2011**, *133*, 2163–2169.

DOI: 10.1021/acsami.7b09386
ACS Appl. Mater. Interfaces 2017, 9, 35218–35225